Progress In Electromagnetics Research, PIER 79, 387–399, 2008

ELECTROMAGNETIC SCATTERING ANALYSIS USING THE TWO-DIMENSIONAL MRFD FORMULATION

M. Gokten

Department of Electrical Engineering and Computer Science
Syracuse University
Syracuse, NY 13244, USA

A. Z. Elsherbeni

Department of Electrical Engineering
The University of Mississippi
University, MS 38677, USA

E. Arvas

Department of Electrical Engineering and Computer Science
Syracuse University
Syracuse, NY 13244, USA

Abstract—Recently developed multiresolution frequency domain (MRFD) technique is applied to two-dimensional electromagnetic scattering problems. Scattered field formulation and perfectly matched layer is implemented into the MRFD formulation. Far field distributions of dielectric and perfectly electric conductor (PEC) bodies are calculated and bistatic echo widths of these structures are presented. Good agreement between MRFD and FDFD results is recognized. It is observed that the MRFD technique demonstrates superior computational efficiency characteristics compared to the traditional FDFD technique.

1. INTRODUCTION

Numerous researchers have extensively used the Finite Difference Frequency Domain (FDFD) technique to analyze electromagnetic scattering problems successfully [1–3]. FDFD presents a mathematically

simple, versatile and extremely stable way of solving Maxwell's equations in the frequency domain, but it generally requires large amounts of computer memory and simulation time. The disadvantages of this method led researchers to develop the MRFD scheme [4, 5], a mathematically intensive technique that consumes computer resources more efficiently, thus requires less computer memory and simulation time.

In this work, the MRFD scheme is further expanded to the analysis of open space problems in the context of scattering from two-dimensional dielectric and PEC bodies. The pure scattered field formulation [6, 7] and Berenger's [8] perfectly matched layer (PML) is implemented into the MRFD formulation.

The efficiency of the MRFD scheme depends on the characteristics of the wavelet base used for the expansion of unknown fields. For an effective MRFD algorithm, the appropriate wavelet base should have certain properties; such as compact support, symmetry, regularity (smoothness) and maximum number of vanishing moments [4]. The MRFD formulation in this work is based on Cohen-Daubechies-Feauveau family of wavelets [9], in particular the CDF (2,2) wavelet, which accommodates all the desired characteristics listed above.

2. FORMULATION

2.1. General Scattered Field Formulation

The formulation developed in this paper is based on the pure scattered field formulation in which the total field is the sum of the known incident and the unknown scattered fields [6, 7]. This formulation evolves from the linearity of Maxwell's equations and the decomposition of the total electric and magnetic fields into an incident field and a scattered field, that is:

$$\vec{E}_{total} = \vec{E}_{inc} + \vec{E}_{scat} \tag{1a}$$

$$\vec{H}_{total} = \vec{H}_{inc} + \vec{H}_{scat}. \tag{1b}$$

The incident field is the field that would exist in the computational domain in which no scatterers exist and therefore satisfies the Maxwell's equations:

$$\nabla \times \vec{E}_{inc} = -j\omega\mu_o \vec{H}_{inc} \tag{2a}$$

$$\nabla \times \vec{H}_{inc} = +j\omega\varepsilon_o \vec{E}_{inc}. \tag{2b}$$

The total fields also satisfy the Maxwell's equations by definition:

$$\nabla \times \vec{E}_{total} = -j\omega\mu \vec{H}_{total} \tag{3a}$$

$$\nabla \times \vec{H}_{total} = +j\omega\varepsilon\vec{E}_{total}. \tag{3b}$$

Using the scattered field decomposition (1), the curl equations (2 and 3) can be combined to yield:

$$\nabla \times \vec{E}_{scat} + j\omega\mu\vec{H}_{scat} = j\omega\left(\mu_o - \mu\right)\vec{H}_{inc} \tag{4a}$$

$$\nabla \times \vec{H}_{scat} - j\omega\varepsilon\vec{E}_{scat} = j\omega\left(\varepsilon - \varepsilon_o\right)\vec{E}_{inc}. \tag{4b}$$

Curl equations (4) can be simplified into three scalar equations for the TM_Z polarized wave which are valid inside the original computational domain (non-PML region):

$$H_{scat,x} + \frac{1}{j\omega\mu_x}\frac{\partial E_{scat,z}}{\partial y} = \frac{\mu_o - \mu_x}{\mu_x}H_{inc,x} \tag{5a}$$

$$H_{scat,y} - \frac{1}{j\omega\mu_y}\frac{\partial E_{scat,z}}{\partial x} = \frac{\mu_o - \mu_y}{\mu_y}H_{inc,y} \tag{5b}$$

$$E_{scat,z} + \frac{1}{j\omega\varepsilon_z}\frac{\partial H_{scat,x}}{\partial y} - \frac{1}{j\omega\varepsilon_z}\frac{\partial H_{scat,y}}{\partial x} = -\frac{\varepsilon_z - \varepsilon_o}{\varepsilon_z}E_{inc,z}. \tag{5c}$$

In order to have a finite computational space, an absorbing boundary condition surrounding the computational space should be implemented to absorb the outgoing waves without reflection. The termination of the computational domain is based on the PML approach. The PML technique is applied by constructing an anisotropic PML absorber just outside the original computational domain. The extended computational domain for a 2D problem is illustrated in Fig. 1. In the two dimensional case, on the left and right side of the computational domain, the absorbing layers only have non-zero conductivity in the x direction, i.e., $\sigma_y^e = 0$ and $\sigma_y^m = 0$. Similarly, the conductivities in the y direction is non-zero on the top and bottom sides. In the four corners all conductivities are non-zero.

Properties of the PML layer have been chosen to effectively absorb all outgoing waves so the theoretical reflection from the PML layer should be zero; however some reflection may occur due to numerical discretization. To reduce this reflection, both electric and magnetic conductivities are chosen to increase from zero at the vacuum-PML interface to a value $\sigma_{\max}$ at the outer layer of the PML. $\sigma_{\max}$ can be determined from [8] as:

$$\sigma_{\max} = -\frac{\varepsilon_0 cn\ln\left[R(0)\right]}{2\delta_{PML}} \tag{6}$$

with n being 1, 2, or 3 for a constant conductivity, a linear conductivity, or a parabolic conductivity profile, respectively. The parameter δ_{PML}

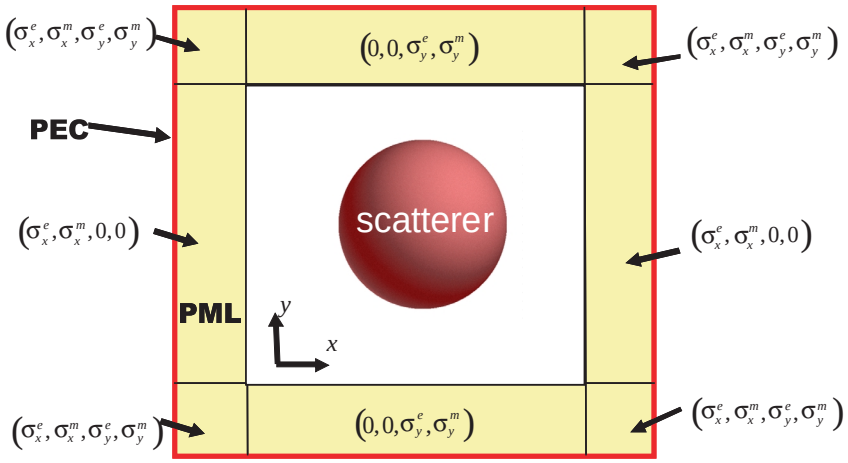

Figure 1. The extended computational domain for 2-D problems.

is the PML layer thickness, c is the speed of light in vacuum, and $R(0)$ is the theoretical reflection factor at normal incidence.

The conductivity distribution inside the absorbing layers can be determined as:

$$\sigma(h) = \sigma_{\max}\left(\frac{h}{\delta_{PML}}\right)^{n+1} \tag{7}$$

where h is the distance from the vacuum-PML interface to a point inside the PML media. These relations make the PML layers a seamless transition from the computational domain to the PEC wall.

Following the notations of [10], inside the PML region, the unsplit-field PML equations can be written as:

$$H_x = \frac{1}{(j\omega\mu_o + \sigma_z^m)}\frac{\partial E_y}{\partial z} - \frac{1}{\left(j\omega\mu_o + \sigma_y^m\right)}\frac{\partial E_z}{\partial y} \tag{8a}$$

$$H_y = \frac{1}{(j\omega\mu_o + \sigma_x^m)}\frac{\partial E_z}{\partial x} - \frac{1}{(j\omega\mu_o + \sigma_z^m)}\frac{\partial E_x}{\partial z} \tag{8b}$$

$$H_z = \frac{1}{\left(j\omega\mu_o + \sigma_y^m\right)}\frac{\partial E_x}{\partial y} - \frac{1}{(j\omega\mu_o + \sigma_x^m)}\frac{\partial E_y}{\partial x} \tag{8c}$$

$$E_x = \frac{1}{\left(j\omega\varepsilon_o + \sigma_y^e\right)}\frac{\partial H_z}{\partial y} - \frac{1}{(j\omega\varepsilon_o + \sigma_z^e)}\frac{\partial H_y}{\partial z} \tag{8d}$$

$$E_y = \frac{1}{(j\omega\varepsilon_o + \sigma_z^e)}\frac{\partial H_x}{\partial z} - \frac{1}{(j\omega\varepsilon_o + \sigma_x^e)}\frac{\partial H_z}{\partial x} \tag{8e}$$

$$E_z = \frac{1}{(j\omega\varepsilon_o + \sigma_x^e)}\frac{\partial H_y}{\partial x} - \frac{1}{\left(j\omega\varepsilon_o + \sigma_y^e\right)}\frac{\partial H_x}{\partial y}. \tag{8f}$$

The 2D TM$_Z$ unsplit-field PML equations which are valid inside the PML region can be obtained from (8) as:

$$H_x + \frac{1}{\left(j\omega\mu_o + \sigma_y^m\right)}\frac{\partial E_z}{\partial y} = 0 \tag{9a}$$

$$H_y - \frac{1}{(j\omega\mu_o + \sigma_x^m)}\frac{\partial E_z}{\partial x} = 0 \tag{9b}$$

$$-E_z + \frac{1}{(j\omega\varepsilon_o + \sigma_x^e)}\frac{\partial H_y}{\partial x} - \frac{1}{\left(j\omega\varepsilon_o + \sigma_y^e\right)}\frac{\partial H_x}{\partial y} = 0. \tag{9c}$$

Two sets of equations, one for the non-PML region (5) and one for the PML region (9) are derived. Since these equations are similar, it is possible to combine them into a single set of equations which is valid in the entirety of the computational space:

$$H_{scat,x} + \frac{1}{j\omega\mu_{xy}}\frac{\partial E_{scat,z}}{\partial y} = \frac{(\mu_o - \mu_{xi})}{\mu_{xi}}H_{inc,x} \tag{10a}$$

$$H_{scat,y} - \frac{1}{j\omega\mu_{yx}}\frac{\partial E_{scat,z}}{\partial x} = \frac{(\mu_o - \mu_{yi})}{\mu_{yi}}H_{inc,y} \tag{10b}$$

$$-E_{scat,z} + \frac{1}{j\omega\varepsilon_{zx}}\frac{\partial H_{scat,y}}{\partial x} - \frac{1}{j\omega\varepsilon_{zy}}\frac{\partial H_{scat,x}}{\partial y} = \frac{(\varepsilon_{zi} - \varepsilon_o)}{\varepsilon_{zi}}E_{inc,z} \tag{10c}$$

The material parameters are distributed differently in the PML and non-PML regions. In the non-PML region the material parameter distribution is described by:

$$\begin{aligned} \mu_{xy} &= \mu_x, \qquad \mu_{yx} = \mu_y \\ \mu_{xi} &= \mu_x, \qquad \mu_{yi} = \mu_y \\ \varepsilon_{zx} &= \varepsilon_{zy} = \varepsilon_{zi} = \varepsilon_z. \end{aligned} \tag{11}$$

The material parameters inside the PML region are:

$$\begin{aligned} \mu_{xy} &= \mu_o + \frac{\sigma_y^m}{j\omega}, \quad \mu_{yx} = \mu_o + \frac{\sigma_x^m}{j\omega} \\ \mu_{xi} &= \mu_o, \quad \mu_{yi} = \mu_o \\ \varepsilon_{zx} &= \varepsilon_o + \frac{\sigma_x^e}{j\omega}, \quad \varepsilon_{zy} = \varepsilon_o + \frac{\sigma_y^e}{j\omega}, \quad \varepsilon_{zi} = \varepsilon_o. \end{aligned} \tag{12}$$

2.2. MRFD Update Equations

In order to generate the MRFD update equations for the TM_Z polarized waves, the computational space should be discretized into cells. The locations of the field vectors and material parameters associated with each cell should be defined. The two-dimensional Yee grid [11] shown in Fig. 2 is used for discretization of the computational domain.

The positions of the field components and material parameters are shown in Fig. 2. All values of ε are associated with electric field components and all values of μ are associated with magnetic field components.

A general 3D MRFD formulation based on the biorthogonal CDF (2,2) wavelet is introduced in [5]. The update equations for 2D waves can be deduced from the 3D update equations of [5] as:

$$H_{scat,x}(i,j) + \frac{1}{j\omega\mu_{xy}(i,j)\Delta y}\sum_{l=1}^{3}a(l)[E_{scat,z}(i,j+l) - E_{scat,z}(i,j-l+1)]$$
$$= \frac{\mu_o - \mu_{xi}(i,j)}{\mu_{xi}(i,j)}H_{inc,x}(i,j) \tag{13a}$$

$$H_{scat,y}(i,j) - \frac{1}{j\omega\mu_{yx}(i,j)\Delta x}\sum_{l=1}^{3}a(l)[E_{scat,z}(i+l,j) - E_{scat,z}(i-l+1,j)]$$
$$= \frac{\mu_o - \mu_{yi}(i,j)}{\mu_{yi}(i,j)}H_{inc,y}(i,j) \tag{13b}$$

$$-E_{scat,z}(i,j) + \frac{1}{j\omega\varepsilon_{zx}(i,j)\Delta x}\sum_{l=1}^{3}a(l)[H_{scat,y}(i+l-1,j) - H_{scat,y}(i-l,j)]$$
$$-\frac{1}{j\omega\varepsilon_{zy}(i,j)\Delta y}\sum_{l=1}^{3}a(l)[H_{scat,x}(i,j+l-1) - H_{scat,x}(i,j-l)]$$
$$= \frac{\varepsilon_{zi}(i,j) - \varepsilon_o}{\varepsilon_{zi}(i,j)}E_{inc,z}(i,j) \tag{13c}$$

where the $a(l)$ coefficients [12] are listed in Table 1.

Table 1. The $a(l)$ coefficients.

l	1	2	3
$a(l)$	1.2291667	−0.0937500	0.0104167

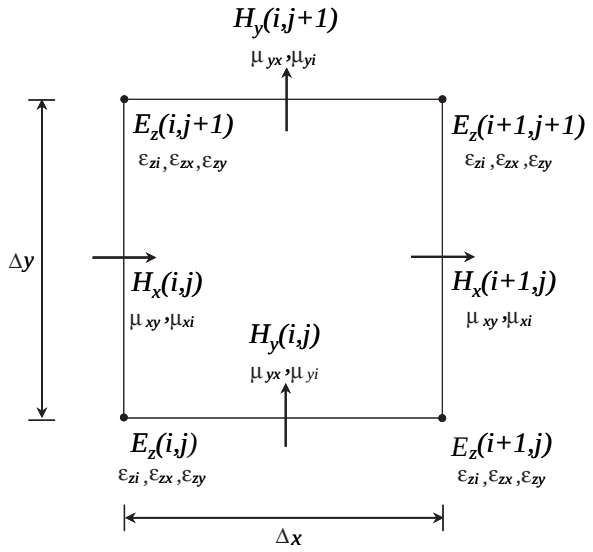

Figure 2. The positions of field components and material parameters on the 2D Yee cell.

2.3. Incident Field Expressions

The TM_Z incident plane wave presented in Fig. 3(a) can be expressed as:

$$\vec{E}_{inc}(\vec{r}) = E_0 \hat{z} e^{-j\vec{k}.\vec{r}} \tag{14}$$

where E_0 specifies the amplitude of the plane wave. The propagation vector $\vec{k}$ and the position vector $\vec{r}$ can be written as:

$$\vec{k} = -k(\cos\phi_{inc}\hat{x} + \sin\phi_{inc}\hat{y}) \tag{15a}$$

$$\vec{r} = x\hat{x} + y\hat{y} \tag{15b}$$

Since the incident field is assumed to be propagating in free space, $k = k_0 = \omega\sqrt{\mu_0\varepsilon_0}$. After the performing the dot product of (15a) and (15b), (14) becomes:

$$\vec{E}_{inc}(\vec{r}) = E_0 \hat{z} e^{jk(x\cos\phi_{inc} + y\sin\phi_{inc})}. \tag{16}$$

The $\vec{H}$ field components can be extracted from the $\vec{E}$ field:

$$\vec{H}_{inc}(\vec{r}) = \frac{1}{\eta}\left[\hat{k} \times \vec{E}(\vec{r})\right]$$

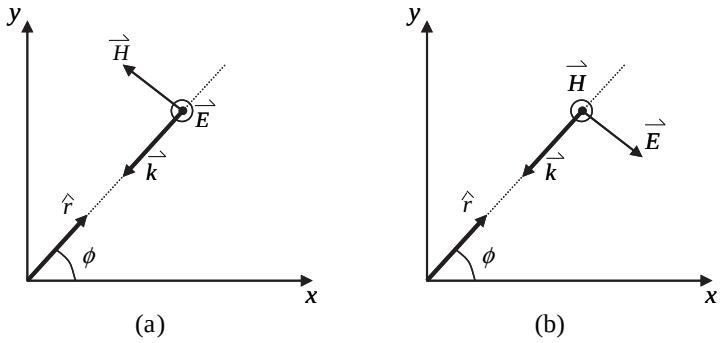

Figure 3. Incident plane waves in a 2D space: (a) TM_Z, (b) TE_Z.

$$= \frac{1}{\eta}E_0\cos\phi_{inc}\hat{y}e^{jk(x\cos\phi_{inc}+y\sin\phi_{inc})} - \frac{1}{\eta}E_0\sin\phi_{inc}\hat{x}e^{jk(x\cos\phi_{inc}+y\sin\phi_{inc})}. \quad (17)$$

In summary, the incident field components for 2D TM_Z problems are:

$$E_{inc,z} = E_0 e^{jk(x\cos\phi_{inc}+y\sin\phi_{inc})} \quad (18a)$$

$$H_{inc,x} = -\frac{1}{\eta}E_0\sin\phi_{inc}e^{jk(x\cos\phi_{inc}+y\sin\phi_{inc})} \quad (18b)$$

$$H_{inc,y} = \frac{1}{\eta}E_0\cos\phi_{inc}e^{jk(x\cos\phi_{inc}+y\sin\phi_{inc})}. \quad (18c)$$

The incident field components for 2D TE_Z wave depicted in Fig. 3(b) can be also obtained in a similar fashion as:

$$H_{inc,z} = H_0 e^{jk(x\cos\phi_{inc}+y\sin\phi_{inc})} \quad (19a)$$

$$E_{inc,x} = \eta H_0\sin\phi_{inc}e^{jk(x\cos\phi_{inc}+y\sin\phi_{inc})} \quad (19b)$$

$$E_{inc,y} = -\eta H_0\cos\phi_{inc}e^{+jk(x\cos\phi_{inc}+y\sin\phi_{inc})}. \quad (19c)$$

3. NUMERICAL RESULTS

The finite difference and multiresolution approaches are applied to the two dimensional problems of scattering of a plane wave from dielectric and PEC cylinders. The fields in the computational domain and

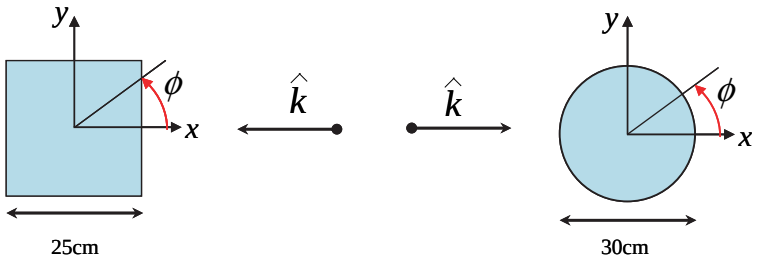

Figure 4. 2D dielectric cylinders illuminated by TM_Z plane wave: (a) square cylinder, (b) circular cylinder.

far field region are calculated and co-polarized bistatic radar cross section for each problem is presented. The source codes are written in MATLAB and executed using a laptop PC with a Pentium M processor at 1.6 GHz. The coefficient matrices are stored in sparse matrices to reduce memory requirements. For all the problems, number of air layers (N_{AIR}) and PML layers (N_{PML}) is set to 4 and 8, respectively and a parabolic variation of conductivity with $R(0) = 10^{-17}$ is used in the PML. For each example, simulation parameters and consumed computer resources are summarized in Table 2.

Table 2. Simulation parameters and computer resources consumed by the two methods.

		Cell Size (mm)	Comp. Space (cells)	Matrix Size (kbyte)	Time (sec)
Square Dielectric Cylinder	FDFD	2.5	124×124	3466	113.9
	MRFD	6.25	64×64	2154	46.1
Circular Dielectric Cylinder	FDFD	2.0	174×174	6757	668.1
	MRFD	5.0	84×84	3733	168.4
Dielectric and PEC Cylinders	FDFD	2.5	424×124	11873	2473.1
	MRFD	6.25	184×64	6295	666.4

First, the problem of scattering from a square dielectric cylinder with $\varepsilon_r = 4$, illustrated in Fig. 4(a), is considered. The width of the square cylinder is 25 cm. The cylinder is illuminated by a 3 GHz

incident TM_Z plane wave with 0° incidence angle off the x-axis. Compared to the FDFD grid with ($\Delta x = \Delta y = 2.5\,\text{mm} = \lambda_{\min}/20$), the MRFD grid is coarser ($\Delta x = \Delta y = 6.25\,\text{mm} = \lambda_{\min}/8$), where $\lambda_{\min}$ is the wavelength inside the scatterer. The scattered co-polarized far field, represented by bistatic echo width, is presented in Fig. 5. Both methods yield similar results, however compared to the finite difference technique, memory and processing time savings of the multiresolution technique is 37.8% and 59.6%, respectively, for the case at hand.

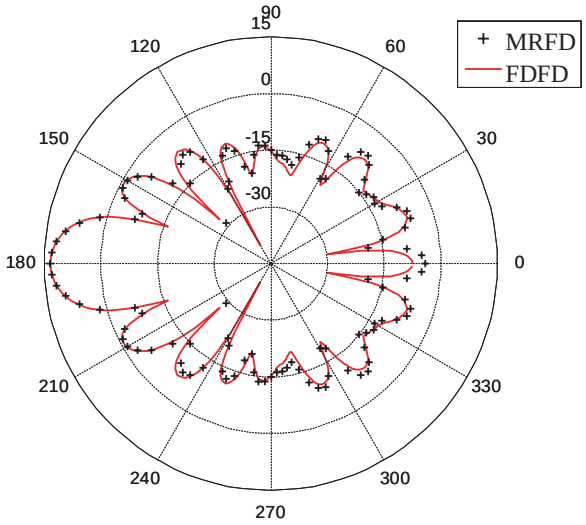

Figure 5. The co-polarized bi-static echo width (σ/λ_o in dB) of the square cylinder illuminated by an incident TM_Z plane wave.

The second example considered is the problem of scattering from a circular dielectric cylinder with $\varepsilon_r = 4$, depicted in Fig. 4(b). The cylinder is illuminated by an incident 3 GHz TM_Z plane wave with 180° incidence angle off the x-axis. The MRFD sampling rate ($\Delta x = \Delta y = 5\,\text{mm} = \lambda_{\min}/10$) is kept low compared to the higher one in the FDFD ($\Delta x = \Delta y = 2\,\text{mm} = \lambda_{\min}/25$). As shown in Fig. 6, there is a good agreement between MRFD and FDFD results. For this case, the memory and processing time savings of the multiresolution technique is 44.8% and 74.8%, respectively.

The last example considered is the problem of scattering from two bodies with different material formation: a square dielectric cylinder with $\varepsilon_r = 4$ and a square PEC cylinder, as illustrated in Fig. 7. The computational domain is excited by a 3 GHz incident TM_Z plane wave with 90° incidence angle off the x-axis.

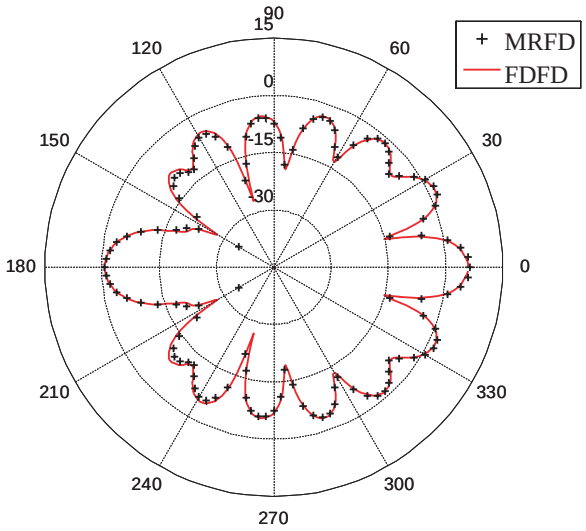

Figure 6. The co-polarized bi-static echo width (σ/λ_o in dB) of the circular cylinder illuminated by an incident TM_Z plane wave.

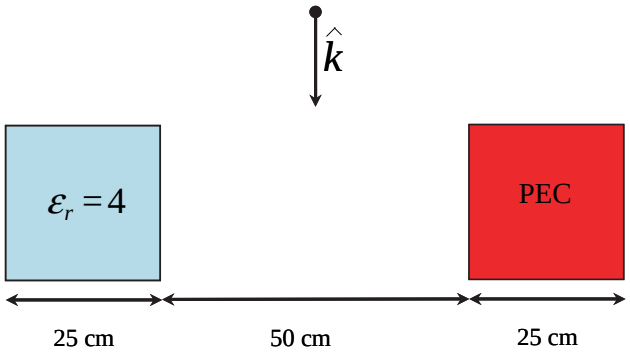

Figure 7. 2D dielectric and PEC cylinders illuminated by TM_Z plane wave.

Again, the far field distribution for the problem is calculated with the MRFD and FDFD techniques. The cell sizes are set to 6.25 mm and 2.5 mm for the MRFD and FDFD lattice, respectively. The scattered co-polarized far field for the problem is shown in Fig. 8. Both methods yielding comparable accuracy, memory and simulation time requirements of the multiresolution technique is 47% and 73% lower than the FDFD.

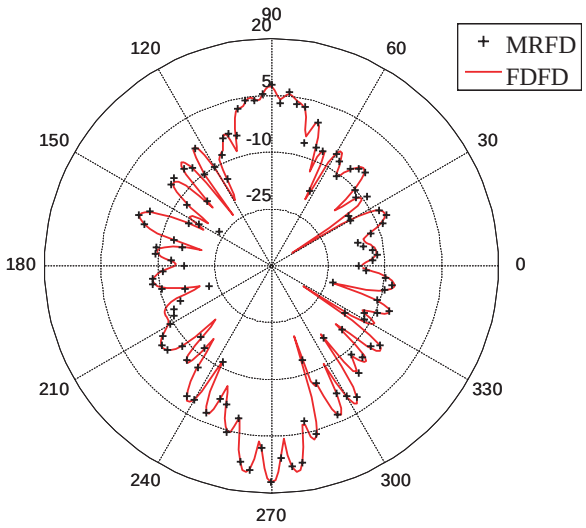

Figure 8. The co-polarized bistatic echo width (σ/λ_o in dB) for the dielectric and PEC squares illuminated by an incident TM_Z plane wave.

4. CONCLUSION

In this work, the multiresolution frequency domain scheme for the scattering analysis of two-dimensional targets is developed. The PML boundary condition and pure scattered field approach is successfully implemented into the MRFD formulation. The newly developed method is validated by analyzing scattering from dielectric and PEC scatterers. The results from MRFD are in good agreement in comparison to the FDFD results. Results indicate that MRFD technique promises substantial savings in terms of execution time and memory requirements.

REFERENCES

1. Sharkawy, M. A., V. Demir, and A. Z. Elsherbeni, "The iterative multi-region algorithm using a hybrid finite difference frequency domain and method of moment techniques," *Progress In Electromagnetics Research*, PIER 57, 19–32, 2006.
2. Kuzu, L., V. Demir, A. Z. Elsherbeni, and E. Arvas, "Electromagnetic scattering from arbitrarily shaped chiral objects

using the finite difference frequency domain method," *Progress In Electromagnetics Research*, PIER 67, 1–24, 2007.

3. Norgren, M., "A hybrid FDFD-BIE approach to two-dimensional scattering from an inhomogeneous biisotropic cylinder," *Progress In Electromagnetics Research*, PIER 38, 1–27, 2002.
4. Gokten, M., A. Z. Elsherbeni, and E. Arvas, "The multiresolution frequency domain method for general guided wave structures," *Progress In Electromagnetics Research*, PIER 69, 55–66, 2007.
5. Gokten, M., A. Z. Elsherbeni, and E. Arvas, "A multiresolution frequency domain method using biorthogonal wavelets," *ACES Conf.*, Miami, FL, 2006.
6. Kunz, K. S. and R. J. Luebbers, *The Finite Difference Time Domain Method for Electromagnetics*, CRC Press LLC, Boca Raton, 1993.
7. Taflove, A. and S. C. Hagness, *Computational Electrodynamics: The Finite-Difference Time-Domain Method*, 3rd ed., Artech House, Boston, MA, 2005.
8. Berenger, J. P., "A perfectly matched layer for the absorption of electromagnetic waves," *Journal of Computational Physics*, Vol. 114, 185–200, 1994.
9. Daubechies, I., *Ten Lectures on Wavelets*, Society for Industrial and Applied Mathematics, Philadelphia, PA, 1992.
10. Al-Sharkawy, M., V. Demir, and A. Z. Elsherbeni, "Iterative Multi-Region Technique for large scale electromagnetic scattering problems — Two dimensional case," *Radio Science*, Vol. 40, No. 5, September 2005.
11. Yee, K. S., "Numerical solution of initial boundary value problems involving Maxwell's equations in isotropic media," *IEEE Transactions on Antennas and Propagation*, Vol. 14, 302–307, 1966.
12. Dogaru, T. and L. Carin, "Multiresolution time-domain algorithm using CDF biorthogonal wavelets," *IEEE Transactions on Microwave Theory and Techniques*, Vol. 49, No. 5, 902–912, May 2001.